Struct Multidisc Optim (2015) 51:1097–1111
DOI 10.1007/s00158-014-1199-3

RESEARCH PAPER

Free material stiffness design of laminated composite structures using commercial finite element analysis codes

A comparison to research code

Søren Randrup Henrichsen · Esben Lindgaard · Erik Lund

Received: 1 April 2014 / Revised: 12 September 2014 / Accepted: 5 November 2014 / Published online: 4 December 2014

Abstract In this work optimum stiffness design of laminated composite structures is performed using the commercially available programs ANSYS and MATLAB. Within these programs a Free Material Optimization algorithm is implemented based on an optimality condition and a heuristic update scheme. The heuristic update scheme is needed because commercially available finite element analysis software is used. When using a commercial finite element analysis code it is not straight forward to implement a computationally efficient gradient based optimization algorithm. Examples considered in this work are a clamped-clamped 2D plate loaded in two load cases and a point loaded six layered 3D double curved corner hinged shell. The first example displays the effect of varying the size of patches having the same parametrization, and the second illustrates the benefit of using a layered free material parametrization. The results provide information concerning topology, material anisotropy, and the direction having the maximum stiffness. The obtained results are compared to gradient based optimization solutions using Discrete Material Optimization and Continuous Fiber Angle Optimization implemented in a research code, where full access to the finite element analysis core is granted. This comparison displays the possibility of using commercially available programs for stiffness design of laminated composite structures.

S. R. Henrichsen (✉) · E. Lindgaard · E. Lund
Department of Mechanical and Manufacturing Engineering, Aalborg University (AAU), Fibigerstræde 16, 9220 Aalborg East, Denmark
e-mail: srh@m-tech.aau.dk

E. Lindgaard
e-mail: elo@m-tech.aau.dk

E. Lund
e-mail: el@m-tech.aau.dk

Keywords Free material optimization · Stiffness design · Laminated composites · Laminate optimization · Commercially available software

1 Introduction

This work considers optimum stiffness design of laminated composite structures using commercially available finite element analysis software. Design of structures using laminated composite materials (here: fiber reinforced polymers) has gained an increasing use in industry when manufacturing high performance structures like aeroplanes and wind turbine blades. The use of composite materials enables the ability to tailor both the material and the structure to the specific loading conditions, thus providing a large design space compared to isotropic materials. Design based on engineering intuition requires much experience, and may result in suboptimal designs. Thus, rational design procedures are needed to assist the designer. These procedures can be used to generate new design suggestions, hereby broadening the design space. Many optimization methods exist for the optimum design of composites, but many of these require full access to the finite element analysis software to be efficient. However, many companies use commercial available finite element software like Abaqus (Dassault Systèmes 2013) and ANSYS (ANSYS Inc 2013b) where access to the backbone of the finite element analysis tool is not granted, thus disabling the possibility of using many gradient based optimization methods efficiently. Commercial optimization tools capable of conducting laminate optimization are available. One program which provides these capabilities is OptiStruct (Altair 2013). The optimization follows a three phase procedure (Zhou et al. 2011; Zhou and Fleury 2012). Phase I is to optimize the thickness of

a predefined set of "superplies", Phase II is to translate the "superplies" into discrete plies, and finally in Phase III the fiber layup is shuffled based on a set of design rules. This method, however, does not take structural bending into account when determining the relative percentage of each "superply". In the research community, many optimization methods exist for design of laminated composite structures. Ghiasi and co-workers (Ghiasi et al. 2009, 2010) provide a comprehensive overview of laminated composite optimization methods for both constant and variable stiffness design. The direct search algorithms constitute one group of methods. Methods in this group include Genetic Algorithms, Particle Swarm Optimization, and Ant Colony Optimization. Common for these is that full access to the finite element analysis software is not necessary. In Bloomfield et al. (2010) a comparison of the state-of-the-art for direct search algorithms is given. Here the Particle Swarm Optimization is shown to provide the best performance of the tested algorithms. However, as the design space increases the effectiveness of the direct search algorithms decreases.

When designing laminated composite structures, the designer is often limited to e.g., a predefined set of sandwich core materials and laminated composite plies oriented in a predefined set of angles. The design task is then to select the optimum material among the available candidates. One method which has proven efficient for solving these kinds of problems is the Discrete Material Optimization (DMO) approach developed by Lund and co-workers (Lund and Stegmann 2005; Stegmann and Lund 2005; Hvejsel and Lund 2011). DMO is a generalization of multiphase topology optimization by Sigmund and Torquato (1997) into any distinct set of materials. However, the DMO method introduces a large amount of design variables, since each candidate material has an individual design variable. To reduce the number of design variables Bruyneel (2011) and Gao et al. (2012) introduce the shape functions with penalization and bi-value coding parametrization methods, respectively. Here each candidate material is given a unique coding. This coding gives a logarithmic increase in the number of design variables, when additional candidate materials are defined.

Relaxing the requirement of the fiber angles such any value is allowable gives a new problem. Optimum orientation of orthotropic materials (here: Continuous Fiber Angle Optimization (CFAO)) constitutes some of the earliest work in optimization of laminated composite structures. Optimal orientation of orthotropic materials is considered in Pedersen (1989), where the optimum angle for orthotropic materials with high and low shear stiffness is derived. Furthermore, Pedersen (1990) derives the bounds on the elastic energy for an orthotropic material assuming a constant strain field, hereby showing the extremum angles and whether it is a minimum or maximum. Later, Cheng and Pedersen (1997) derived the sufficient conditions for optimal orientation of orthotropic materials under stiffness considerations. Thomsen and Olhoff (1990) extended the work by Pedersen (1989, 1990) to encompass orientation and fiber concentration of a laminate having three orthogonal plies. Bruyneel and Fleury (2002) conduct stiffness optimization of laminated composite structures considering both fiber angles and ply thickness as design variables. In Abrate (1994) a review of different formulations for CFAO is presented, these formulations display optimization strategies for stiffness, linear buckling, thermal, eigenfrequency, and multicriteria optimization.

The DMO and CFAO approaches are based on the use of predefined materials, whereas Free Material Optimization (FMO) is used to design the optimum constitutive properties. Furthermore, FMO can be regarded as a relaxation of topology optimization, where both the topology within the domain is determined, but also the optimum constitutive parameters for the domains with material. The initial work in FMO is conducted in Ringertz (1993) and by Bendsøe and co-workers (Bendsøe et al. 1994; 1995; 1996). Common for these two approaches is that the resulting problem is a convex positive semi-definite problem, where the constitutive matrix is symmetric. Ringertz (1993) used the entries in the full symmetric constitutive matrix as design variables resulting in 6 design variables for 2D problems per design domain. This parametrization is used by Kočvara et al. (2008) as a part of the PLATO-N research project (PLATO-N 2013). One focus point of the project work was to develop semi-definite programming methods applicable for FMO. Furthermore, free material formulations for compliance and stress criteria are presented in the paper by Kočvara et al. (2008). Bendsøe et al. (1994) generalized the work by Pedersen (1989, 1990) and showed that the optimum free material is orthotropic with the principal material directions aligned and scaled with respect to the principal strains. This reduces the optimization task to determine the material stiffness multiplier throughout the design domain. Recently, Pedersen and Pedersen (2013) extended this work by defining an upper bound on the stiffness, hereby changing the design variables into topology variables. This parametrization changes the stiffness distribution problem from Bendsøe et al. (1994) into a material distribution problem. None of the presented FMO formulations impose any constraints on the material except for (semi-)positive definiteness of the constitutive stiffness matrix, thus solutions from FMO must be post processed before these can be used for manufacturing. Hörnlein et al. (2001) use an initial FMO design for subsequent post processing into fiber paths for manufacturing using a tape laying machine.

In this work, an optimization framework is presented based on a commercially available finite element analysis software. The optimization process should rely on quantities which are available from the finite element analysis software for efficiency. As an example, the design sensitivities for eigenfrequency and compliance topology optimization can be determined using the strain energy and kinetic energy, see Kim and Kim (2000). From this efficient gradient based optimization can be conducted. However, as the sensitivity of each component in the constitutive matrix is needed for gradient based FMO, and since these cannot be extracted directly the sensitivities must be determined using finite difference approximations. This requires several calls to the finite element analysis software, rendering such a method inefficient. Instead, the optimization is based on an optimality criterion using a heuristic update scheme. A stiffness optimality criterion is considered within the current framework. The optimization is build into an ANSYS-MATLAB environment. These programs are considered being industry standard programs. Within these programs FMO is implemented based on the work by Pedersen and Pedersen (2013). This work is extended to accommodate patches and multilayered structures. Multilayered structures provide information concerning the required bending stiffness of a structure. Numerical examples will display the capabilities of the implemented optimization method. The results obtained are compared to results from the gradient based optimization methods DMO and CFAO. DMO and CFAO are implemented within the special purpose analysis and optimization research code MUST (the MUltidisciplinary Synthesis Tool) developed at the Department of Mechanical and Manufacturing Engineering at Aalborg University (MUST 2014). The outcome of these examples displays the capabilities of using optimality criteria and heuristic update methods for the design of laminated composite structures if commercially available finite element analysis software is used.

The remainder of the paper is organized as follows; in Section 2 we present the FMO formulation and implementation hereof. A presentation of the gradient based algorithms DMO and CFAO is given in Section 3. The implemented FMO formulation is compared to DMO and CFAO through two examples in Sections 4 and 5, and finally we sum up the findings in Section 6.

2 Free material optimization; formulation and implementation

The basis for the results obtained in Sections 4 and 5 is presented in this and in the following section. First the maximum stiffness (or minimum compliance) optimization problem is presented. Equations (1a–d) displays the minimum compliance problem.

$$\min_{y_k} \quad C = \mathbf{d}^T\mathbf{f} = \mathbf{d}^T\mathbf{K}\mathbf{d} \tag{1a}$$

$$\text{s.t.} \quad \mathbf{f} = \mathbf{K}\mathbf{d} \tag{1b}$$

$$M \leq \overline{M} \tag{1c}$$

$$\underline{y_k} \leq y_k \leq \overline{y_k} \tag{1d}$$

Here C is the compliance of the structure, $\mathbf{d}$ and $\mathbf{f}$ are the global displacement and load vectors, respectively. The global stiffness matrix is represented by $\mathbf{K}$, M and $\overline{M}$ are the current and maximum allowable mass of the system, respectively. Lastly y_k, $\underline{y_k}$, and $\overline{y_k}$ represent a set of generalized design variables and bounds which will be defined for FMO, DMO, and CFAO individually. Equation (1b) is not directly included into the optimization problem, but will be solved explicitly when needed, thus a nested analysis and design approach is used (Arora and Wang 2005).

In this work so-called patches will be used. Here, this defines a group of elements which is forced to have the same properties with respect to material properties and fiber orientation. The advantage of using patches is the possibility of having a fine finite element discretization while limiting the number of design variables.

2.1 Free material optimization

The free material optimization formulation is based on the work by Pedersen and Pedersen (2013), and is in this work extended to encompass patches and layered structures. The formulation is based on a combination of topology optimization and the optimum orthotropic material from Bendsøe et al. (1994). The optimum orthotropic material defines the relative constitutive parameters in a unit norm anisotropy matrix, and the topology variable determines whether material is present or not. This resulting anisotropy matrix is multiplied by a free material scalar stiffness constituting the upper bound on the stiffness for the material. The generalized design variables y_k are the topology variables within the patches, and will be denoted by x_s. Due to the single design variable per patch, the FMO formulation is easily implemented in a heuristic update scheme based on the optimality criterion: if the strain energy density is constant throughout the structure, it is the stiffest possible. This optimality criterion is derived by Prager and Taylor (1967) for a single load case and no bounds on the design variables, and will here

be applied for bounded design variables and multiple load cases.

In the following, we will show the FMO formulation by Pedersen and Pedersen (2013) extended to encompass patches and multilayered structures. A plane stress assumption is applied during the optimization. The used update scheme only takes inplane effects into account, consequently this will only provide suboptimal designs. This method was tested in Pedersen (2006) where it is shown that the designs obtained using this assumption are close to those where out of plane effects are considered. The following terms will be used throughout the description of the FMO formulation; the subset of patches for which the topology variable is not at the boundaries is defined as the free patches i.e., $\underline{x_s} < x_s < \overline{x_s}$. A quantity of this subset will be denoted by the notation $\tilde{}$. Inner and outer iterations can be defined using Fig. 1. The inner iterations are performed in the box denoted [B] where the new set of topology variables are determined, these iterations are denoted by j. The outer iterations are related to the closed loop constituted by the boxes [C]-[A]-[B], and is denoted by i.

The basis of the FMO formulation is the optimum orthotropic material $\boldsymbol{\alpha}_{12}$ originally derived by Bendsøe et al. (1994) and shown in (2). It defines the optimum material properties in the local principal strain coordinate system.

$$\boldsymbol{\alpha}_{12,e,l} = \frac{1}{\epsilon_{1,e,l}^2 + \epsilon_{2,e,l}^2} \begin{bmatrix} \epsilon_{1,e,l}^2 & \epsilon_{1,e,l}\epsilon_{2,e,l} & 0 \\ \epsilon_{1,e,l}\epsilon_{2,e,l} & \epsilon_{2,e,l}^2 & 0 \\ 0 & 0 & 0 \end{bmatrix} \tag{2}$$

Here $\epsilon_{\{1,2\},e,l}$ is the first or second principal strain in element e for load case l. $\boldsymbol{\alpha}_{12,e,l}$ defines the element anisotropy matrix in the element inplane principal strain 1-2 coordinate system. The trace and Frobenius norm of the $\boldsymbol{\alpha}_{12,e,l}$ matrix are equal to 1, see (2). These anisotropy matrices are rotated into the element inplane structural x-y coordinate system, and in order to construct the anisotropic matrix for patch s, $\boldsymbol{\alpha}_{xy,s}$, a weighted sum over the anisotropy matrices is conducted:

$$\boldsymbol{\alpha}_{xy,s} = \frac{1}{\sum_{e=1}^{n^e}\sum_{l=1}^{n^l} u_{e,l}} \sum_{e=1}^{n^e}\sum_{l=1}^{n^l} u_{e,l}\boldsymbol{\alpha}_{xy,e,l} \tag{3}$$

Here $u_{e,l}$ is the strain energy density for element e and load case l. n^l is the number of load cases and the sum $e = 1, \ldots, n^e$ is the sum over the elements in patch s. The inner loop is shown in Algorithm 1. This loop updates the topology variables.

Algorithm 1 Inner loop for updating topology variables.

1: $j = 1$
2: Initialize: $F^1 = 1$, dV^1 some large number
3: Calculate: $\tilde{V}^1 = \sum_{s=1}^{n^s} \begin{cases} x_{s,i}^{FE} V_s & : \underline{x_s} < x_{s,i}^{FE} < \overline{x_s} \\ 0 & : \text{otherwise} \end{cases}$
4: **while** $\left|\frac{dV^j}{\tilde{V}^j}\right| > 10^{-11}$ **do**
5: $j = j + 1$
6: Calculate: $x_{s,i}^j = x_{s,i}^{FE} \left(\frac{\breve{u}_s}{\tilde{\breve{u}}}\right)^q F^{j-1} \quad \forall\, s$
7: Calculate: $\tilde{V}^j = \sum_{s=1}^{n^s} \begin{cases} x_{s,i}^j V_s & : \underline{x_s} < x_{s,i}^j < \overline{x_s} \\ 0 & : \text{otherwise} \end{cases}$
8: Calculate: $dV^j = \sum_{s=1}^{n^s} \left(x_{s,i}^j - x_{s,i}^{FE}\right) V_s$
9: **if** $\tilde{V}^j = 0$ **or** $\tilde{V}^j + dV^j \leq 0$ **then**
10: **repeat**
11: Calculate: $x_{s,i}^j = x_{s,i}^{FE} + 0.95(x_{s,i}^j - x_{s,i}^{FE})$
12: Calculate: $\tilde{V}^j$ and dV^j
13: **until** $\tilde{V}^j \neq 0$ **and** $\tilde{V}^j + dV^j > 0$
14: **end if**
15: Calculate: $F^j = F^{j-1}\frac{\tilde{V}^j}{\tilde{V}^j + dV^j}$
16: **end while**
17: $x_{s,i+1}^{FE} = x_{s,i}^j$

In the algorithm $x_{s,i}^{FE}$ is the topology variable for outer iteration i in patch s. $\breve{u}_s$ is the maximum of the strain energy densities over all load cases in patch s, and $\tilde{\breve{u}}$ is the mean of all the free $\breve{u}_s$. To dampen fluctuations in the design variable update, a constant q is introduced and given a value below 1. F^j scales the topology variables $x_{s,i}^j$ such the total change in volume $dV^j \approx 0$, hence F^j can be interpreted as a kind of Lagrange multiplier for the mass constraint (Pedersen and Pedersen 2013). Since the mass constraint is implicitly controlled by securing that the change in volume is negligible between two outer iterations, it is important to initialize the topology variables such the mass constraint is fulfilled. $\tilde{V}$ is the sum of all free volumes and dV is the total change in volume. The work-wise of the algorithm is as follows; F^1 is initialized to 1 because the mass constraint initially is fulfilled. dV^1 is given a sufficiently large number such $\left|\frac{dV^j}{\tilde{V}^j}\right| > 10^{-11}$ and the while loop on line 4 is entered. The while loop secures that the change in mass between two outer iterations is sufficiently low i.e., $dV \approx 0$, thus fulfilling the mass constraint. The first step in the loop is to determine a new temporary set of topology variables $x_{s,i}^j$. This is based on the assumption that an increase in topology variable will result in a decrease in strain energy density and vise-verse. From this set of design variables the free volume and the change in volume are calculated, and F^j is updated. The update of F^j is based on a proper scaling between the remaining (free) volume $\tilde{V}$ and the change in volume dV. In lines 8 to 13 a check of the temporary design variables is implemented. This is done to secure a positive value for the denominator in F^j, since a negative

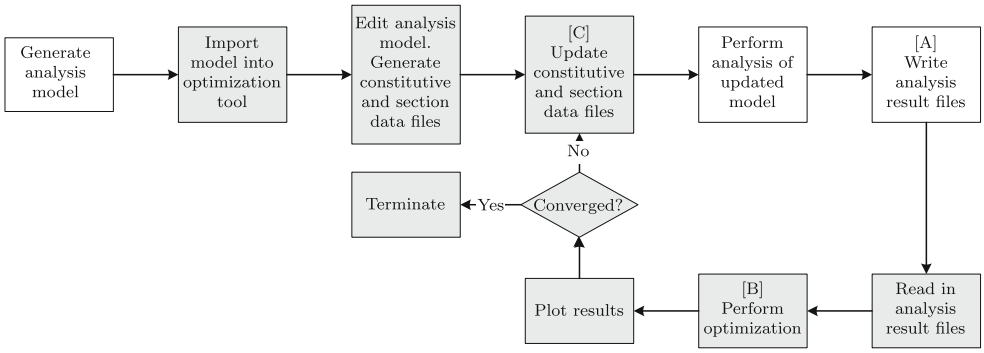

Fig. 1 Flowchart of optimization procedure using ANSYS and MATLAB environment. *White boxes* are performed in ANSYS, *gray* in MATLAB

value will result in $x_{s,i}^{j} = \underline{x_s}$ for all s. If this is the case, we recommend a relaxation of the temporary design change as: $x_{s,i}^{j} = x_{s,i}^{FE} + 0.95(x_{s,i}^{j} - x_{s,i}^{FE})$ to avoid the aforementioned problem. When the algorithm has converged, the temporary set of topology variables is accepted, and the design variables $x_{s,i+1}^{FE}$ are updated. The updated topology variables, $x_{s,i+1}^{FE}$, are used to update the constitutive matrix $\mathbf{E}_{s,i+1}$ in a two step procedure. The first step is to calculate an intermediate constitutive matrix $\hat{\mathbf{E}}_s$ based on the updated topology variables and the anisotropy matrices calculated in (3). However, as the applied update scheme has no information of prior outer iterations a constant β is introduced in the second step. This limits the design change between two outer iterations, and the resulting constitutive matrix is given in (5).

$$\hat{\mathbf{E}}_s = \mathbf{E}_0 + w(x_{s,i+1}^{FE}) E_F \boldsymbol{\alpha}_{xy,s} \tag{4}$$

$$\mathbf{E}_{s,i+1} = \beta \hat{\mathbf{E}}_s + (1-\beta)\mathbf{E}_{s,i} \tag{5}$$

In (4) $\mathbf{E}_0$ is a low stiffness material which ensures positive definiteness for $\hat{\mathbf{E}}_s$, E_F is the free material stiffness, and w is a weighting function for the topology variable given as, see Pedersen and Pedersen (2013) for details:

$$w(x_s) = r_4 (1 - t(x_s)) t(x_s) + t(x_s)^2 \tag{6}$$

where:

$$\begin{aligned} t(x_s) &= r_1 - \sqrt{r_2 + r_3 x_s} \\ r_1 &= \tfrac{k_1 - 1}{k_0 + k_1 - 2} & r_2 &= r_1^2 \\ r_3 &= \tfrac{k_0 - k_1}{k_0 + k_1 - 2} & r_4 &= 2k_0 \tfrac{1 - k_1}{k_0 - k_1} \end{aligned}$$

Here k_0 and k_1 are the slopes of the interpolation function at $x_s = 0, 1$, respectively. The bounds on x_s are given as $\underline{x_s} = 10^{-3}$ and $\overline{x_s} = 1$, respectively. Finally, Pedersen and Pedersen (2013) define a measure of the anisotropy, A_s, of a patch. The anisotropy is determined by rotating the constitutive matrix $\mathbf{E}_{s,i+1}$ counterclockwise with steps of $\frac{\pi}{1800}$ [rad] between 0 [rad] and π [rad], and selecting the first (if multiple) angle ϕ which maximizes entrance (1,1). This stiffness entrance is divided by the trace of the matrix as in (7).

$$A_s \equiv \frac{E_{11,s,i+1}^{\phi}}{\mathrm{Tr}\left(\mathbf{E}_{s,i+1}^{\phi}\right)} \tag{7}$$

Since E_{11} is maximized A_s has a value in the interval [1/3;1]. Additionally, A_s is a measure of the properties of the strain field within a patch. If the strain field is highly unidirectional, A_s is approaching 1 and the resulting material only has stiffness in one direction. If the strain field is highly varying within a patch, A_s will approach 1/3, thus a material with equal shear and normal stiffnesses is approached. The multilayered FMO formulation relies on the same equations as the single layered formulation. The only difference between the two formulations is that each step must be conducted layer-wise.

2.2 Implementation

For the optimization using ANSYS and MATLAB an interface is programmed. The MATLAB code is used to update the analysis model and get the new model response from ANSYS. The full simulation flow is depicted on Fig. 1. Most of the work is conducted in MATLAB as seen on Fig. 1, since the optimization is performed herein along with the update of the model. ANSYS is called once per outer iteration, and it is only used to evaluate the updated model and output the relevant model data i.e., the layer principal strains (and stresses in the case of a multilayered formulation), element principal angles, the layer strain energy densities, and layer volumes for each layer in the model.

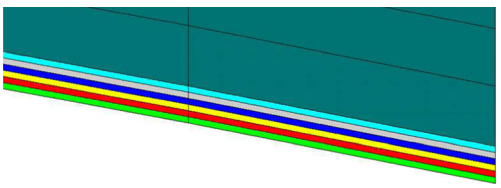

Fig. 2 Sketch of stacked solid elements, the *colors* define the individual layers/elements

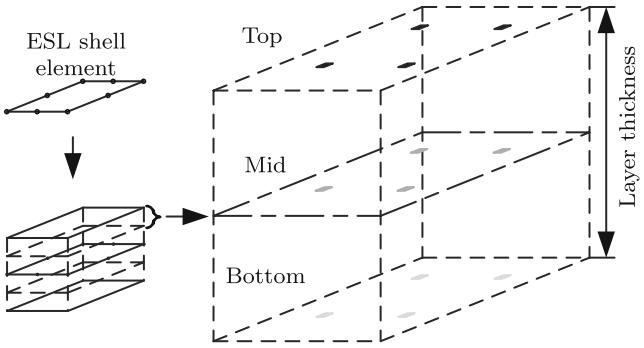

Fig. 3 Sketch of integration of shell layers, parallelograms display points where the stresses and strains are calculated. *Top*, *Mid*, and *Bottom* defines the top, middle, and bottom part of a layer, respectively

Composite structures rarely consist of a single layer so a multilayered finite element model is needed. Applying a multilayered FMO formulation provides information concerning the required bending stiffness. This information would not be available when using a single layer model. One way of modeling a layered structure is to stack solid elements where one element represent one layer, see Fig. 2. Consequently, this results in a model having many degrees of freedom, which quickly becomes inefficient. Another method is to use equivalent single layer (ESL) elements. Here the layers are assumed to be perfectly bonded together, such that the strains are continuous through the laminate thickness. Using shell elements only the geometrical mid-plane is modeled, hereby the model is more efficient. However, in ANSYS volumes and strain energies are considered being element quantities and cannot be extracted layer-wise. Thus, for layered elements these data must be computed in MATLAB. It is chosen to use the super convergent Gauss Point stresses and strains to calculate the strain energy densities. These Gauss Point strain energy densities are then averaged to form top, middle, and bottom strain energy densities for each layer. Subsequently, the strain energy

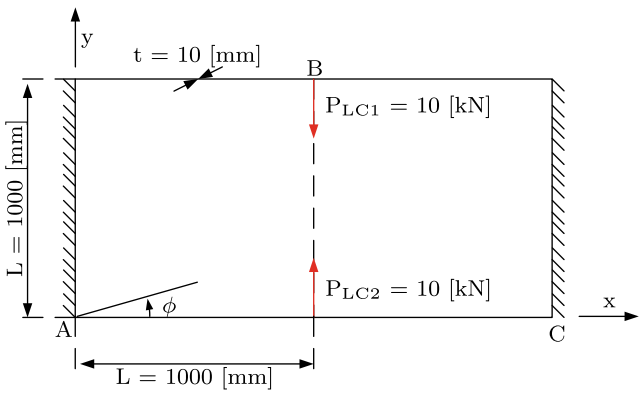

Fig. 4 Boundary conditions and dimensions for clamped-clamped plate. ϕ defines the rotation angle for the fibers

Table 1 Material properties used for the clamped-clamped plate and corner hinged shell

Parameter		GFRP	Foam	FM
E_x, E_F	[GPa]	38.0	0.148	38.0
E_y, E_z	[GPa]	9.0	0.148	–
G_{xy}, G_{xz}	[GPa]	3.60	0.05	–
G_{yz}	[GPa]	3.46	0.05	–
ν_{xy}, ν_{xz}, ν_{yz}	[–]	0.3	0.48	–
ρ	$\left[\frac{\text{kg}}{\text{m}^3}\right]$	1870	130	1870

densities for the entire layer, u_e, is calculated by averaging previous calculated strain energy densities employing a Simpson-based integration scheme, see Fig. 3 (ANSYS Inc 2013a). The result of this has been verified by comparison with results from ANSYS by calculating the total and element strain energy for a structure similar to the layered corner hinged shell presented in Section 5.

3 Sensitivity based methods

This section provides a short summary of the DMO and CFAO methods along with the design sensitivity analysis. For a more thorough description of the methods we refer to the provided references. The optimization problem in (1a–d) is used as the basis for the methods, and is solved using sequential linear programming with a global convergence filter based on Chin and Fletcher (2003). The sensitivities of the objective function and constraints are needed in order to update the design. As the mass constraint is linear in or independent of the design variables the mass sensitivities are not shown. For compliance minimization problems having design independent loads, it is advantageous to calculate the sensitivity of the objective function using the adjoint approach described in e.g., Bendsøe and Sigmund (2003). The result is restated here.

$$\frac{\mathrm{d}C}{\mathrm{d}y_s} = -\sum_{e=1}^{n^e} \mathbf{d}_e^T \frac{\mathrm{d}\mathbf{K}_e}{\mathrm{d}y_s} \mathbf{d}_e \quad \forall s \tag{8}$$

Here $\mathbf{K}_e$ and $\mathbf{d}_e$ are the element stiffness matrix and displacement vector for element e in patch s, respectively. Furthermore, the derivative of the element stiffness matrix is given as:

$$\frac{\mathrm{d}\mathbf{K}_e}{\mathrm{d}y_s} = \int_{V_e} \mathbf{B}^T \frac{\mathrm{d}\mathbf{E}_s}{\mathrm{d}y_s} \mathbf{B} \, \mathrm{d}V \tag{9}$$

Here $\mathbf{B}$ is the strain-displacement matrix and V_e is the element volume. The derivative of the constitutive matrix is needed to conduct gradient based optimization using DMO and CFAO. This is evident from (9).

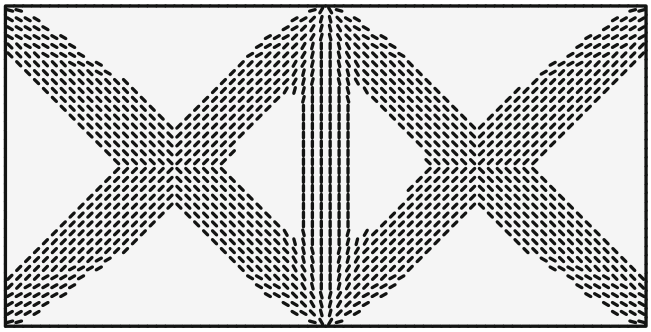

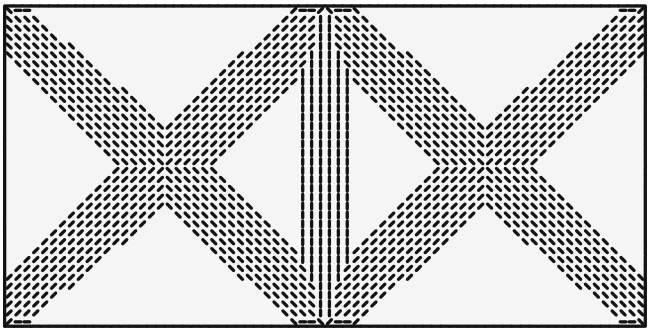

Fig. 5 DMO results for clamped-clamped plate having 72 × 36 patches and material constraint of 50 %. *Left*: 13 candidate materials, *Right*: 5 candidate materials

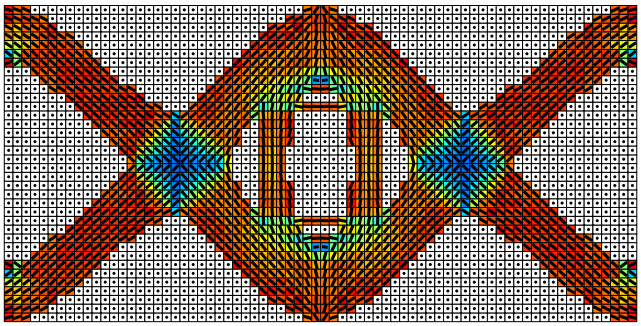

Fig. 6 FMO result for clamped-clamped plate having 72 × 36 patches and material constraint of 50 %

3.1 Discrete material optimization

The basic idea of the DMO approach is to convert the discrete problem of selecting the best candidate material to a continuous problem where weighting functions with penalization are used to obtain a distinct choice of material. Candidate materials are often layers of composites aligned at different orientations and sandwich core materials, but all materials can be used as long as the stiffness matrices between these are distinct. The DMO scheme used is the "Solid Isotropic Material with Penalization" (SIMP) based scheme generalized to multi-phase topology optimization with orthotropic materials as presented in Hvejsel and Lund (2011). As for all DMO schemes, the generalized design variables y_k are the candidate material densities x_c. Having this formulation the constitutive matrix $\mathbf{E}_s$ for patch s is given by:

$$\mathbf{E}_s = \mathbf{E}_0 + \sum_{c=1}^{n^c} x_{c,s}^p \Delta \mathbf{E}_{c,s} \quad \forall s \tag{10}$$

Here $\Delta \mathbf{E}_{c,s} = \mathbf{E}_{c,s} - \mathbf{E}_0$, $\mathbf{E}_{c,s}$ is candidate c in the patch, n^c is the number of candidate materials, and p is the SIMP penalization factor. Since the SIMP weighting functions are not self balancing an extra constraint is introduced which controls the total amount of candidate material available in a domain.

$$\sum_{c=1}^{n^c} x_{c,s} = 1 \quad \forall s \tag{11}$$

Thus, $x_{c,s}$ can be considered as volume fractions of the associated candidate materials. Lastly, the sensitivity of the constitutive matrix needed in (9) is given by:

$$\frac{\mathrm{d}\mathbf{E}_s}{\mathrm{d}x_{c,s}} = p x_{c,s}^{p-1} \Delta \mathbf{E}_{c,s} \quad \forall c, s \tag{12}$$

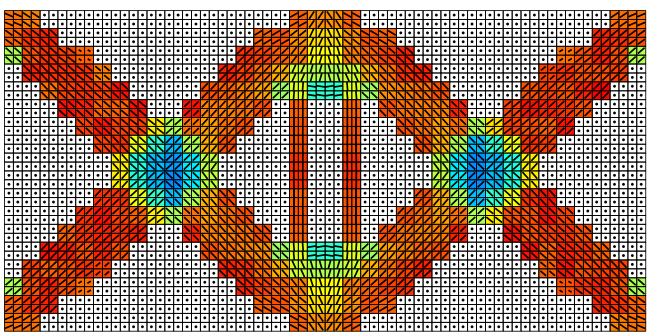

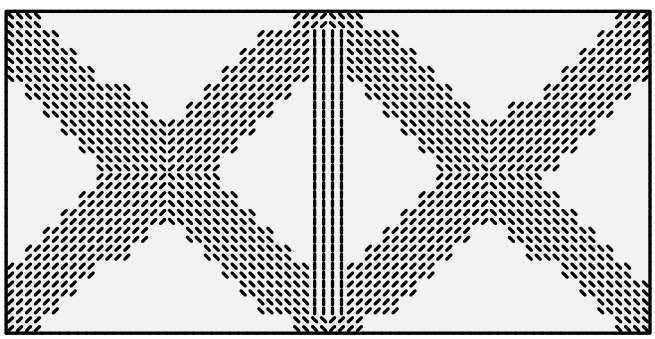

Fig. 7 Result for clamped-clamped plate having 36 × 18 patches and material constraint of 50 %. *Left*: FMO, *right*: DMO

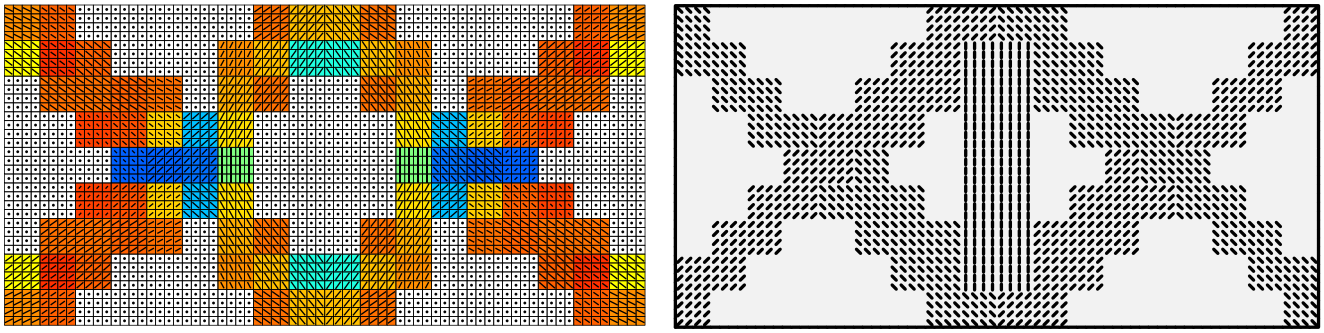

Fig. 8 Result for clamped-clamped plate having 18 × 9 patches and material constraint of 50 %. *Left*: FMO, *right*: DMO

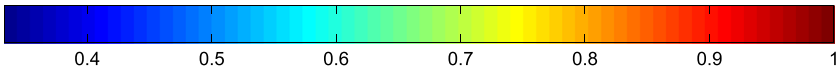

Fig. 9 Color index of anisotropy for free material, GFRP ≈ 0.75

Using this method the bounds on the candidate materials x_c can be chosen as: $0 \leq x_c \leq 1$.

3.2 Continuous fiber angle optimization

CFAO is a standard gradient-based fiber angle optimization algorithm. This implies that no material distribution is possible while using this method, thus only the stiff orthotropic material is present. The task of the optimization is to rotate the material into the angle ϕ which minimizes the objective function, thus the generalized design variables y_k are the rotation angles ϕ_s of the orthotropic material within patch s. The sensitivity of the constitutive matrix $\mathbf{E}_s$ is calculated using central difference approximations. The bounds on the design variables ϕ_s are chosen such that these will not be reached during the optimization. This is done by choosing $\underline{\phi_s} < \phi_0 - 180°$ and $\phi_0 + 180° < \overline{\phi_s}$ where ϕ_0 is the initial fiber angle.

4 Clamped-clamped plate

In the first example we consider a clamped-clamped plate loaded by two independent load cases of equal importance and loads of equal magnitude. The plate is considered as a 2D problem and is shown on Fig. 4. This plate has previously been studied by Bendsøe et al. (1995) and is here used to compare results from FMO, DMO, and CFAO for a multiple load case scenario. At the same time, the effect of varying the patch size is shown.

The plate is discretized using 72 × 36 quadratic elements. Through convergence studies, this mesh is found to yield a sufficient representation of the structural response and the constitutive properties. The number of patches is either 72 × 36, 36 × 18, or 18 × 9. The material properties are displayed in Table 1. A Glass Fiber Reinforced Polymer (GFRP) is used as a stiff orthotropic material for DMO and CFAO, FM represents the free material, and when a material constraint is imposed the foam material is used

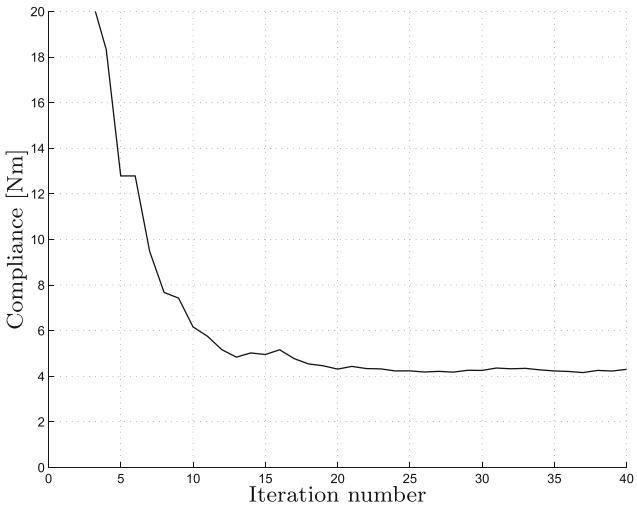

Fig. 10 Optimization history for compliance of the free material optimized clamped-clamped plate having 72 × 36 patches. The convergence limit is $\max(\Delta x_s) < 0.01$. 40 iterations are used before convergence

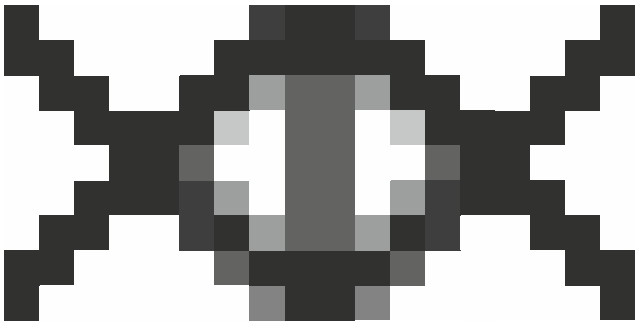

Fig. 11 Convergence of material for DMO having 18 × 9 patches. *White*: Foam, *Black*: GFRP, *gray*: Not converged

as the compliant material. Hence, the low stiffness material is a foam material, so the "white" elements which in classical topology optimization represent void material here represent an isotropic material which still has load carrying capability. In this work the compliance values are not compared since the same stiffness is not available in the two material models. This can be realized by constructing the plane stress reduced stiffness matrix for GFRP (here $\mathbf{E^G}$) using the data in Table 1, see e.g., Jones (1999), and the free material using (2) and (4) with $\mathbf{E_0} = \mathbf{0}$, $w = 1$. Selecting $\{\epsilon_1, \epsilon_2\} = \{\sqrt{E^G_{11}/E^G_{22}}, 1\}$ gives an equal ratio between entrance (1,1) and (2,2) in the two plane stress reduced stiffness matrices, respectively. The two matrices are given in (13).

$$\begin{aligned} \mathbf{E^G} &= \begin{bmatrix} 38.8 & 2.8 & 0 \\ 2.8 & 9.2 & 0 \\ 0 & 0 & 3.6 \end{bmatrix} \text{ [GPa]} \\ \mathbf{E^{FM}} &= \begin{bmatrix} 30.7 & 15.0 & 0 \\ 15.0 & 7.3 & 0 \\ 0 & 0 & 0 \end{bmatrix} \text{ [GPa]} \end{aligned} \tag{13}$$

Evident from the equation is that a simple scaling of the free material stiffness E_F cannot provide a free material which represents the GFRP. Additionally, in the free material no shear stiffness is present, and rotation of the free material stiffness matrix such that the shear stiffness is raised will result in non-zero shear-extension couplings which are not present in GFRP. Consequently, only the topologies and the fiber angles are compared through the structure.

4.1 Comparison of FMO and DMO

In the comparison between FMO and DMO a material constraint of maximum 50 % of the stiff material is imposed since both of these methods are capable of optimizing the topology. For FMO the material properties are directly interpolated between foam and free material using (4). A total of five DMO candidate materials are available; GFRP with the possible orientations of $\{0°, \pm 45°, 90°\}$ constitutes four of the candidates while the foam constitutes the fifth. This number of candidate materials is sufficient for representing the optimum topology and fiber distribution for the plate. A comparison of the optimum topology and fiber distribution using 13 candidate materials (GFRP aligned at $\{0°, \pm 15°, \pm 30°, \pm 45°, \pm 60°, \pm 75°, 90°\}$ and foam) and the selected five candidate materials is shown on Fig. 5. Negligible differences are observed in the obtained designs. Furthermore, all the presented results have been compared to results obtained using 9 (GFRP aligned at $\{0°, \pm 30°, \pm 45°, \pm 60°, 90°\}$ and foam) and 13 candidate materials to secure the validity of the previous conclusion.

The results obtained from the different patch sizes are shown on Figs. 5, 6, 7, and 8. Similar topologies are obtained both when varying the patch size and switching between FMO and DMO. The topology is composed of two arches combining e.g., the points A-B-C on Fig. 4. Furthermore, a reinforcement is present at the center region for the models having 72 × 36 and 36 × 18 patches. These results fit well with the result from Bendsøe et al. (1995). On the figures depicting the FMO results black lines represent the maximum stiffness direction used in (7), and in

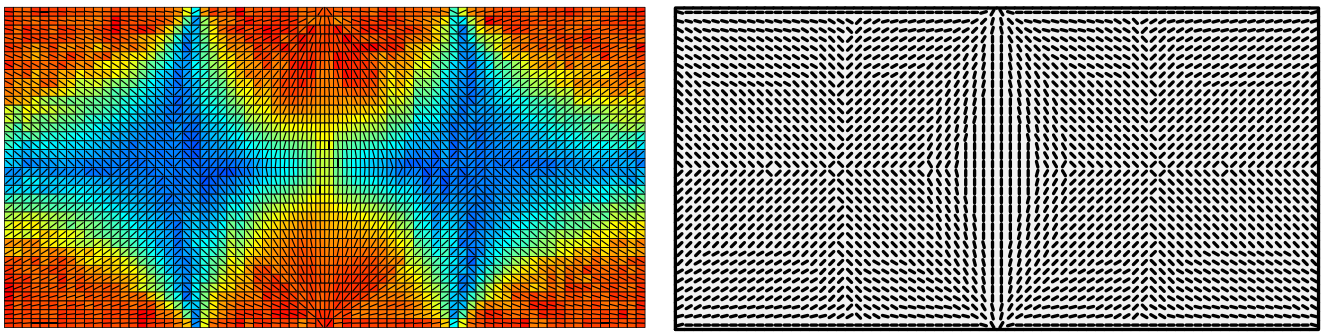

Fig. 12 Result for clamped-clamped plate having 72 × 36 patches and no material constraint. *Left*: FMO, *right*: DMO having 12 candidate materials i.e., GFRP aligned at $\{0°, \pm 15°, \pm 30°, \pm 45°, \pm 60°, \pm 75°, 90°\}$

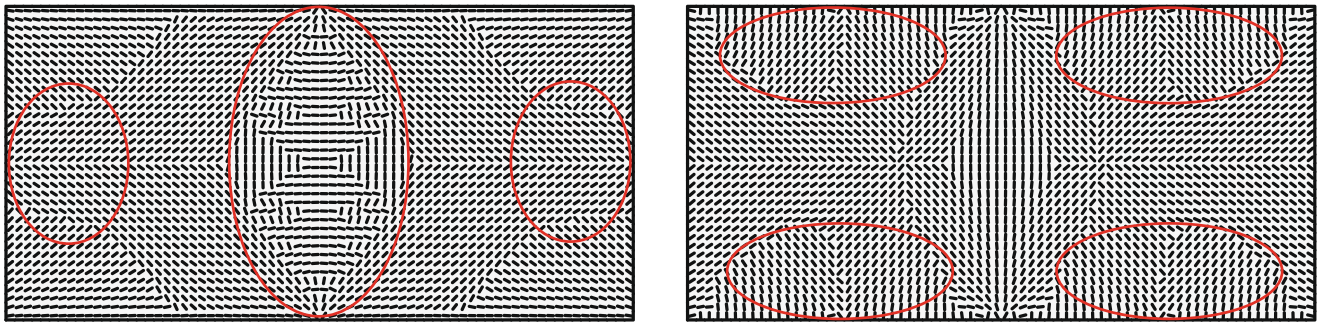

Fig. 13 Effect of initial angle, ϕ_0, for CFAO. The *red circles* display the areas where main differences from the FMO result on Fig. 12 appear. *Left*: Initial angle 0°, *right*: Initial angle 90°

the remainder of the paper these are referred to as fiber angles. Additionally, the colors on the figures give the corresponding value of the anisotropy visualized for all FMO results. The color index for the anisotropy is shown on Fig. 9. For GFRP an estimate of the anisotropy can be calculated by (14).

$$A_{GFRP} \equiv \frac{E_{11}^G}{E_{11}^G + E_{22}^G + E_{66}^G} = \frac{E_x}{E_x + E_y + \left(1 - \nu_{xy}\nu_{yx}\right) G_{xy}} \approx 0.75 \qquad (14)$$

Here E_{ij}^G are the plane stress reduced stiffnesses. ν_{yx} is the minor Poisson's ratio. A_{GFRP} corresponds to a yellow color by comparison of this value to Fig. 9, so the anisotropy for GFRP is optimum only at a minority of the structure. For the 72 × 36 patch models shown on Figs. 5 and 6 the optimum fiber angles are similar for the two optimization methods. The center sections for FMO and DMO are different since the FMO result has two bars, whereas DMO only has one. This difference is a consequence of the materials used by FMO and DMO shown in (13). The anisotropy of the FMO results shows that the structure primarily consist of material having highly unidirectional properties. The exception is in the area where the two arches coincide, here the anisotropy drops to a value around 0.5. In these areas a bi-axial ply or an isotropic material would constitute a good material choice in stead of the uni-directional GFRP used for the presented DMO parameterization due to the loading conditions. It should be noted that the areas with unidirectional properties (red) resemble the anisotropy of a carbon fiber reinforced polymer which has an anisotropy of approximately 0.9 assuming $E_x = 137.9$ [GPa], $E_y = 9.0$ [GPa], $G_{xy} = 7.1$ [GPa], and $\nu_{xy} = 0.3$. For both FMO and DMO the fiber angles are primarily oriented approximately at ±45° and 90°. The 90° fibers are used in the center region, and the ±45° fibers are used in the rest of the structure. On Fig. 10 the optimization history for the compliance of the 72 × 36 patch plate is depicted. As expected the compliance is decreasing as the iteration number is increased until a value of approximately 4 [Nm] is reached, whereafter the compliance of the structure cannot be lowered further and the convergence limit: $\max(\Delta x_s) < 0.01$ is reached. Throughout the iterations the total volume of the free material is not changing significantly. A change in volume of $1.5 \cdot 10^{-12}$ between iteration 1 and 40 is observed when normalizing with the element volume.

For the 36 × 18 patch model the resulting topologies and fiber directions are displayed on Fig. 7, and here the

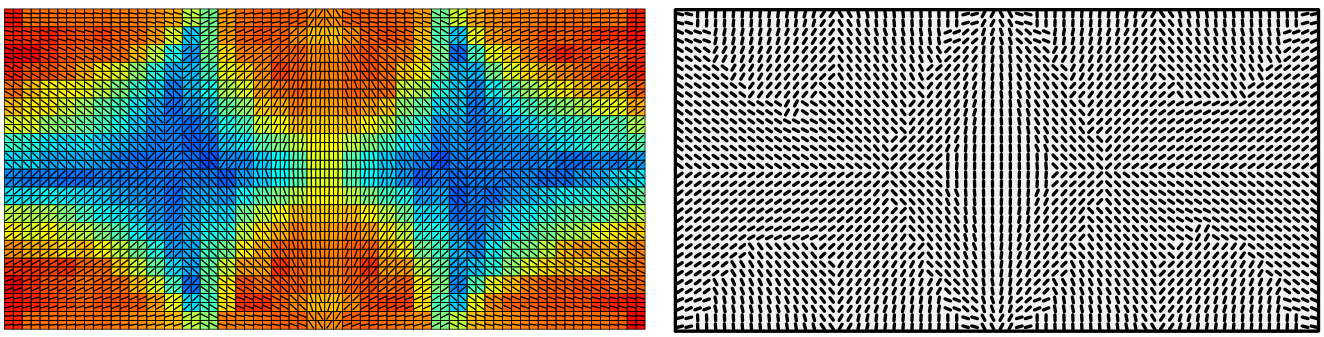

Fig. 14 Result for clamped-clamped plate having 36 × 18 patches and no material constraint. *Left*: FMO, *right*: CFAO

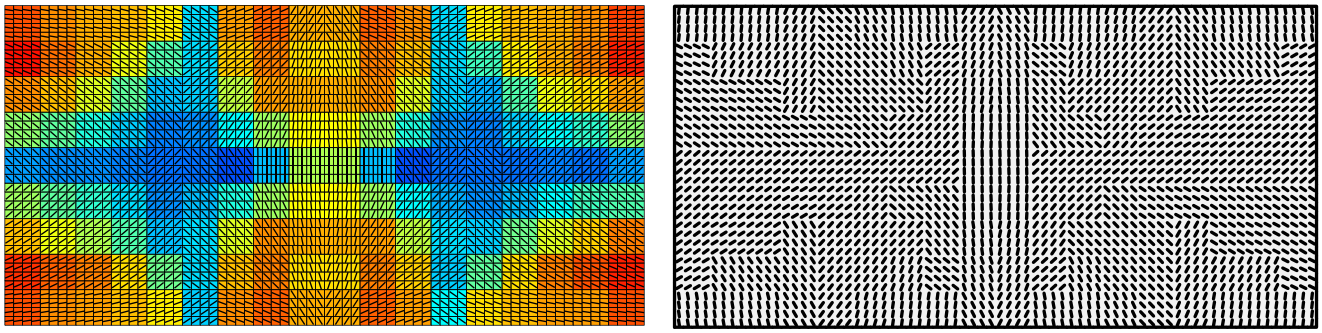

Fig. 15 Result for clamped-clamped plate having 18 × 9 patches and no material constraint. *Left*: FMO, *right*: CFAO

same tendencies as for the 72 × 36 models are observed. However, material is moved from the center region to the arches. This is done in order to compensate for the larger patches in the structure.

On Fig. 8 the results from the 18 × 9 patch models are depicted. Not enough material is present to result in a pure candidate selection for the DMO approach for the coarse model. This is seen on Fig. 11 where the convergence of the candidate materials is depicted as an interpolation between white (foam) and black (GFRP), thus gray displays a patch which is not converged to a distinct material choice. Consequently, a large part of the structure has converged to an intermediate material containing a mixture of the candidates. The cause of this is the combination of patch size and material constraint. A unique choice of material could be obtained by using penalty methods to prevent intermediate-valued designs as described in Hvejsel et al. (2011). However, as patches with intermediate design values provide valuable information regarding the best anisotropy for the given patch, this has not been performed.

The general level of anisotropy for the FMO results is lower when the patch size is raised. The cause of this is that more elements are grouped within the patches which allow for a possible larger variation of the strain field within the patches, consequently, the result is a free material with lower anisotropy.

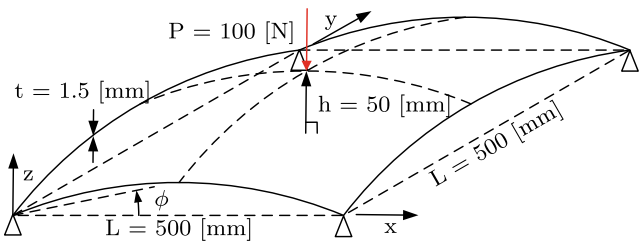

Fig. 16 Boundary conditions and dimensions for corner hinged shell. ϕ defines the inplane rotation angle for the fibers

4.2 Comparison of FMO and CFAO

In the second part FMO is compared to CFAO. Only stiff material is present in the design domain. Consequently, the resulting fiber angles are optimized, and for FMO also the anisotropy. Since CFAO is known to provide different results based on the initial angle, ϕ_0, the effect of the initial fiber angle is evaluated by choosing an initial angle of either 0° or 90°, and optimizing the 72 × 36 patch model. The results are compared to the optimum fiber angles using FMO and DMO (12 GFRP candidate materials). The results from the optimizations are depicted on Figs. 12 and 13 for FMO and DMO and CFAO, respectively. The resulting fiber angles for FMO and DMO are in good agreement, which is shown on Fig. 12. The red circles on Fig. 13 display the areas where the CFAO results are different from the fiber angles obtained using FMO. Furthermore, the angles from CFAO are close to perpendicular to the corresponding FMO fiber angles, which is a consequence of the initial angle. The differences in the optimum fiber angles for the CFAO results lead to different compliance values. The stiffest design is obtained with an initial angle of 90°, therefore, the CFAO results used as a basis of comparison for the remainder of the paper are based on the results having an initial fiber angle of 90°.

The same patch sizes as in Section 4.1 are used. On Figs. 12, 13, and 15 the results are shown. For all patch sizes regardless of the optimization method some tendencies can be observed; in the center region the fibers are aligned at 90°, and most of the remaining fibers are aligned at approximately ±45°. The 72 × 36 patch models are depicted on Figs. 12 and 13. As stated previously the differences in the fiber angles between the methods are present at the corners and at the load introductions. Regardless, CFAO produces a symmetrical design, which is not the case for FMO, which is slightly non-symmetric due to the method used when determining the fiber angle. Additionally, the structure optimized using FMO consists of material having

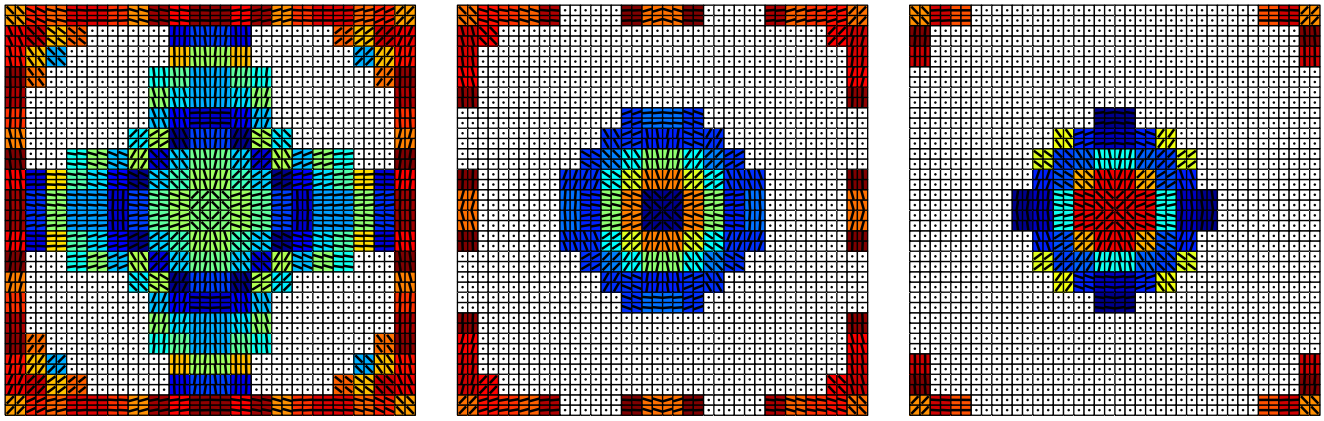

Fig. 17 Result for layer 1 (*bottom*) to 3 of the corner hinged shell optimized using FMO

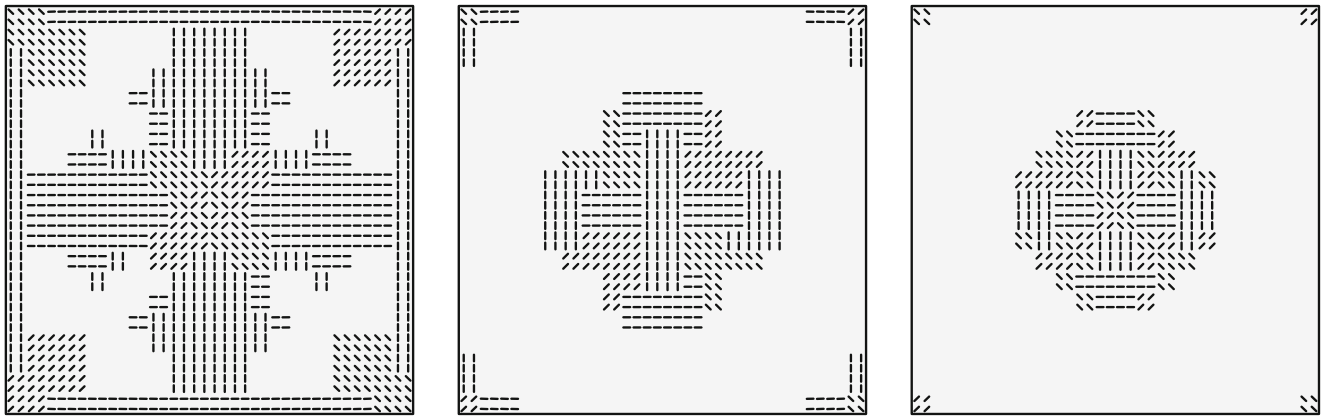

Fig. 18 Result for layer 1 (*bottom*) to 3 of the corner hinged shell optimized using DMO

anisotropy similar to and below that of GFRP. As expected, this is the case in areas where both load cases are having similar influence. Furthermore, compared to the cases with a material constraint large areas contain material with lower anisotropy. This is due to the difference in topology, where the topologies in e.g., Fig. 6 consist of a beam like

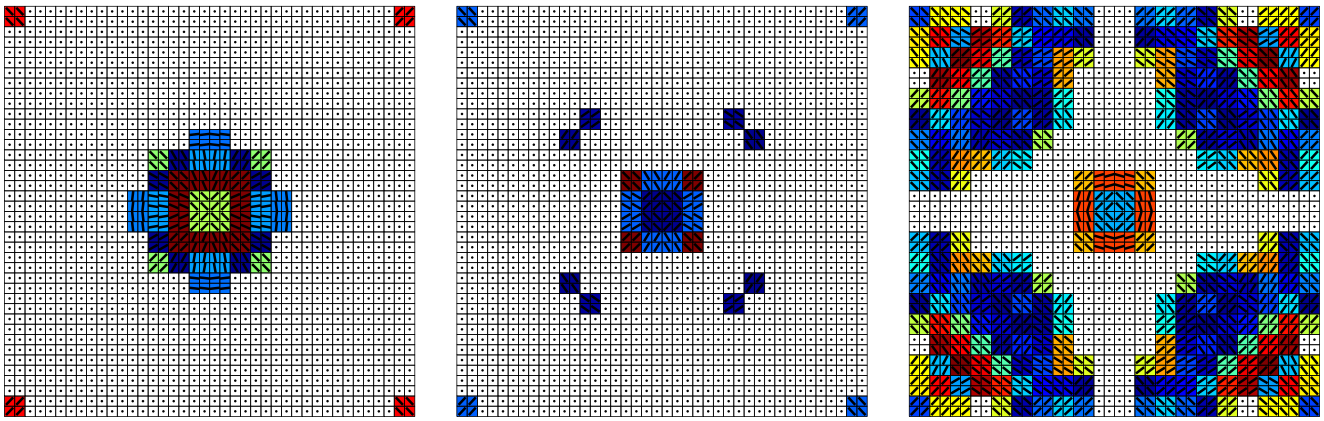

Fig. 19 Result for layer 4 to 6 (*top*) of the corner hinged shell optimized using FMO

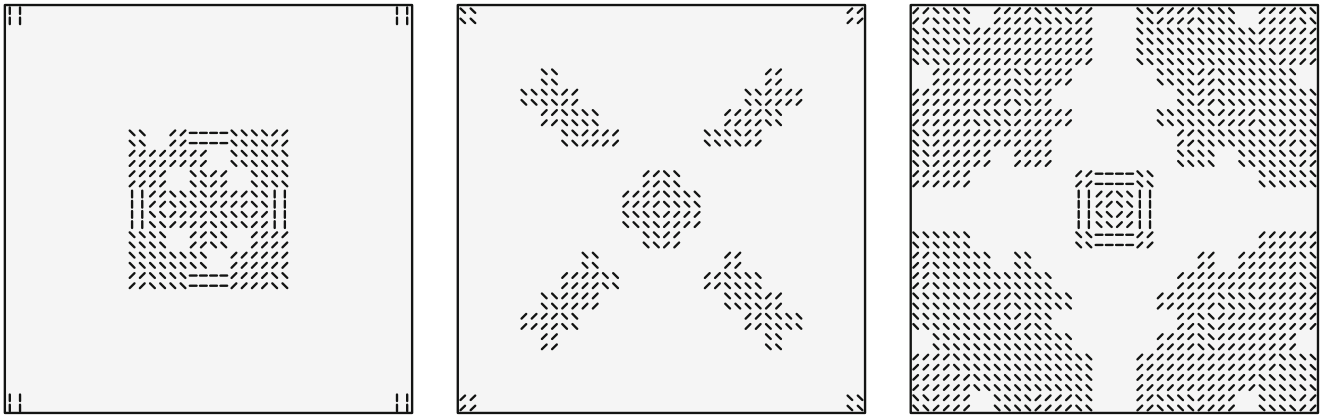

Fig. 20 Result for layer 4 to 6 (*top*) of the corner hinged shell optimized using DMO

structure primarily loaded in a single direction as opposed to the full material plates, where larger areas are loaded bidirectionally.

For the 36 × 18 patch models shown on Fig. 14 similar conclusions as for the 72 × 36 model can be made, just with the difference that the model has a coarser graduation of the contours due to the 2 × 2 element patch size. On Fig. 15 the coarse 18 × 9 patch results are depicted. As with the other models good coherency between the fiber angles exist. Furthermore, the general level of anisotropy is lower than for the models having more patches. This supports the conclusion from Section 4.1.

These comparisons demonstrate the possibility of conducting stiffness design optimization of laminated composites by FMO for 2D structures using a commercial finite element analysis code. Additionally, the examples have illustrated multiple load case problems and the effect of varying patch size. In the following a multilayered shell structure is considered using the commercial environment.

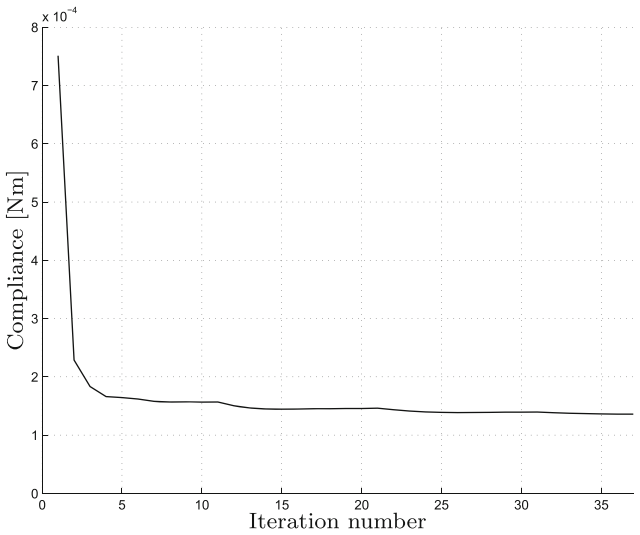

Fig. 21 Optimization history for compliance of free material optimized corner hinged shell. The convergence limit is $\max(\Delta x_s) < 0.005$. 37 iterations are used before convergence

5 Corner hinged shell

The second example is a square corner hinged shell having the dimensions and boundary conditions as depicted on Fig. 16. The surface of the shell can be described using $z(x, y) = h - (2h/L^2)((x - L/2)^2 + (y - L/2)^2)$. For the second test case, the size of the patch is fixed, and the layered formulation is used. To optimize the structure FMO and DMO are used. The shell is modeled using 40 × 40 9-noded ESL shell elements employing a First-order Shear Deformation Theory. The shell consists of 6 layers and 20 × 20 patches per layer. The material properties from Table 1 are used and the same five DMO candidates as in Section 4 are available. Optimization using the DMO approach with 9 and 13 candidate materials has been conducted, and the resulting topologies are similar to the topology obtained using 5 DMO candidate materials, hence, only results from the 5 candidate model are shown. The structure is restricted to contain at least 65 % foam material.

On Figs. 17, 18, 19, and 20 the results from the FMO and DMO optimizations are shown. Here layer 1 represents the bottom layer and layer 6 the top layer. The shell is primarily loaded in bending, so the stiff material is mainly located at the outer layers for both methods in order to provide bending stiffness. The stiff material is located at the center region and at the supports for the inner layers. The results obtained using DMO are not completely symmetric in-plane. This is due to the mass constraint of at least 65 % foam material which with the applied parametrization does not result in

a completely symmetric design. Assuming a polar coordinate system with origin at the center of the shell the fiber angles are primarily oriented in the radial or circumferential direction for FMO and for DMO a candidate material with an orientation close to these directions. Comparing the anisotropy of the shell, Figs. 17 and 19, to the plate given in Fig. 7, it is observed that the general level of anisotropy is lower for the shell than for the plate. The optimization history for the compliance of the corner hinged shell is shown on Fig. 21 for the free material optimized case. Convergence is reached within 37 iterations where the convergence limit: $\max(\Delta x_s) < 0.005$ is reached. The compliance is rapidly dropping to a value of approximately $1.5 \cdot 10^{-4}$ [Nm]. As this value is reached the change in compliance between two iterations decreases. The relative change in volume between the first and last iteration is $3 \cdot 10^{-13}$.

From this example the benefit of a multilayered Free Material Optimization is evident, since the variety in topology, fiber angle, and anisotropy between the layers is significant, rendering it difficult to interpret an equivalent single layered FMO model into a similar laminate configuration.

In this section it is demonstrated that the implemented code is also capable of determining designs for multilayered structures and obtaining designs similar to DMO available in a research code. We have shown that a simple heuristic method implemented in a commercial environment can be used to design multilayered laminated composite structures for stiffness.

6 Conclusion

In this study we have implemented Free Material Optimization in an ANSYS-MATLAB environment in order to demonstrate the capabilities of performing stiffness design optimization of laminated composite structures using commercially available finite element analysis codes. An optimality criteria based approach has been applied in the design optimization using a heuristic update scheme due to the restrictions in access to the finite element backbone in ANSYS. This approach is used to minimize the compliance of the considered structures. Examples considered in this work are; a single layered plate having multiple load cases and a multilayered shell. In the first example the effect of grouping elements into patches suitable for manufacturing of laminated composite structures is considered, whereas for the second example the benefits of using a multilayered Free Material Optimization formulation is demonstrated. The results obtained are compared to results using Discrete Material Optimization and Continuous Fiber Angle Optimization approaches implemented in the in-house research code MUST (the MUltidisciplinary Synthesis Tool) (MUST 2014). Through the study it is concluded that the results obtained from the commercial and the research codes are similar with respect to topology and optimum fiber angles. From this it is apparent that commercial codes can be used to generate initial stiffness design estimates of laminated composite structures which can aid the designer during the design phase. This enables the possibility for applying optimum design procedures for laminated composite structures without the access to a special purpose research code.

Furthermore, the use of Free Material Optimization allows the designer to assess the optimum material stiffnesses to be used throughout the structure, thus providing valuable knowledge in the initial design phase.

Acknowledgments This research is sponsored by The Danish National Advanced Technology Foundation (DNATF) Grant no. 107-2012-2. This support is gratefully acknowledged.

References

Abrate S (1994) Optimal design of laminated plates and shells. Compos Struct 29(3):269–286

Altair (2013) Altair OptiStruct. http://www.altairhyperworks.com/

ANSYS Inc (2013a) ANSYS Release 14.0 Documentation

ANSYS Inc (2013b) ANSYS web page., http://ansys.com/

Arora J, Wang Q (2005) Review of formulations for structural and mechanical system optimization. Struct Multidiscip Optim 30(4):251–272

Bendsøe M, Sigmund O (2003) Topology optimization: theory, methods and applications, 2nd edn. Springer-Verlag, Berlin

Bendsøe MP, Guedes JM, Haber RB, Pedersen P, Taylor JE (1994) An analytical model to predict optimal material properties in the context of optimal structural design. J Appl Mech 61(4):930–937

Bendsøe MP, Diaz AR, Lipton R, Taylor JE (1995) Optimal design of material properties and material distribution for multiple loading conditions. Int J Numer Methods Eng 38(7):1149–1170

Bendsøe MP, Guedes JM, Plaxton S, Taylor JE (1996) Optimization of structure and material properties for solids composed of softening material. Int J Solids Struct 33(12):1799–1813

Bloomfield MW, Herencia JE, Weaver PM (2010) Analysis and benchmarking of meta-heuristic techniques for lay-up optimization. Comput Struct 88(5–6):272–282

Bruyneel M (2011) SFP-a new parameterization based on shape functions for optimal material selection: application to conventional composite plies. Struct Multidiscip Optim 43(1):17–27

Bruyneel M, Fleury C (2002) Composite structures optimization using sequential convex programming. Adv Eng Softw 33(7–10): 697–711

Cheng G, Pedersen P (1997) On sufficiency conditions for optimal design based on extremum principles of mechanics. J Mech Phys Solids 45(1):135–150

Chin CM, Fletcher R (2003) On the global convergence of an SLP-filter algorithm that takes EQP steps. Math Programm 96(1):161–177

Dassault Systèmes (2013) Abaqus Unified FEA. http://www.3ds.com/products-services/simulia/portfolio/abaqus/overview/

Gao T, Zhang W, Duysinx P (2012) A bi-value coding parameterization scheme for the discrete optimal orientation design of the composite laminate. Int J Numer Methods Eng 91(1): 98–114

Ghiasi H, Pasini D, Lessard L (2009) Optimum stacking sequence design of composite materials Part I: constant stiffness design. Compos Struct 90(1):1–11

Ghiasi H, Fayazbakhsh K, Pasini D, Lessard L (2010) Optimum stacking sequence design of composite materials Part II: variable stiffness design. Compos Struct 93(1):1–13

Hörnlein H, Kočvara M, Werner R (2001) Material optimization: bridging the gap between conceptual and preliminary design. Aerosp Sci Technol 5(8):541–554

Hvejsel C, Lund E (2011) Material interpolation schemes for unified topology and multi-material optimization. Struct Multidiscip Optim 43(6):811–825

Hvejsel CF, Lund E, Stolpe M (2011) Optimization strategies for discrete multi-material stiffness optimization. Struct Multidiscip Optim 44(2):149–163

Jones RM (1999) Mechanics of composite materials, 2nd edn. Materials Science and Engineering Series. Taylor & Francis Group

Kim TS, Kim YY (2000) Mac-based mode-tracking in structural topology optimization. Comput Struct 74(3):375–383

Kočvara M, Stingl M, Zowe J (2008) Free material optimization: recent progress. Optimization 57(1):79–100

Lund E, Stegmann J (2005) On structural optimization of composite shell structures using a discrete constitutive parametrization. Wind Energy 8(1):109–124

MUST (2014) The MUltidisciplinary Synthesis Tool. Department of Mechanical and Manufacturing Engineering, Aalborg University, http://www.must.m-tech.aau.dk/

Pedersen NL (2006) On design of fiber-nets and orientation for eigenfrequency optimization of plates. Comput Mech 39(1):1–13

Pedersen P (1989) On optimal orientation of orthotropic materials. Struct Optim 1(2):101–106

Pedersen P (1990) Bounds on elastic energy in solids of orthotropic materials. Struct Optim 2(1):55–63

Pedersen P, Pedersen NL (2013) On strength design using free material subjected to multiple load cases. Struct Multidiscip Optim 47(1):7–17

PLATO-N (2013) A platform for topology optimisation incorporating, novel large-scale, free-material optimisation and mixed integer programming methods. http://www.plato-n.org/

Prager W, Taylor J (1967) Problems of optimal structural design. J Appl Mech 35:102–106

Ringertz U (1993) On finding the optimal distribution of material properties. Struct Optimization 5(4):265–267

Sigmund O, Torquato R (1997) Design of materials with extreme thermal expansion using a three-phase topology optimization method. J Mech Phys Solids 45(6):1037–1067

Stegmann J, Lund E (2005) Discrete material optimization of general composite shell structures. Int J Numer Methods Eng 62(14):2009–2027

Thomsen J, Olhoff N (1990) Optimization of fiber orientation and concentration in composites. Control Cypernetics 19(3–4):321–341

Zhou M, Fleury R (2012) Composite optimization – Ply drop-rate constraints for concept and detailed design. In: Proceeding of the 23rd international congress of theoretical and applied mechanics (ICTAM). Beijing, China

Zhou M, Fleury R, Kemp M (2011) Optimization of composite - recent advances and application. In: Proceeding of the 7th altair CAE technology conference. Warwickshire, United Kingdom